Research Article Vol. 5, No. 9 / September 2018 / Optica 1150

Super-resolution quantum imaging at the Heisenberg limit

Manuel Unternährer,[1] Bänz Bessire,[1] Leonardo Gasparini,[2] Matteo Perenzoni,[2] and André Stefanov[1,*]

[1]Institute of Applied Physics, University of Bern, 3012 Bern, Switzerland
[2]Fondazione Bruno Kessler FBK, 38122 Trento, Italy
*Corresponding author: andre.stefanov@iap.unibe.ch

Received 14 May 2018; revised 3 July 2018; accepted 20 August 2018 (Doc. ID 326641); published 20 September 2018

The Abbe–Rayleigh diffraction limit constrains spatial resolution for classical imaging methods. Quantum imaging exploits correlations between photons to reproduce structures with higher resolution. Quantum-correlated N-photon states were shown to potentially surpass the classical limit by a factor of $1/N$, corresponding to the Heisenberg limit, using a method known as optical centroid measurement (OCM). In this work, the theory of OCM is reformulated for its application in imaging. Using entangled photon pairs and a recently developed integrated time-resolving detector array, OCM is implemented in a proof-of-principle experiment that demonstrates the expected enhancement. Those results show the relevance of entanglement for imaging at the Heisenberg limit.

OCIS codes: (270.0270) Quantum optics; (350.5730) Resolution; (190.4410) Nonlinear optics, parametric processes; (270.5570) Quantum detectors; (040.1240) Arrays.

https://doi.org/10.1364/OPTICA.5.001150

1. INTRODUCTION

In metrology, the optimal measurements of a parameter under restricted use of limited measurement resources are studied [1–3]. Using N independent particles for probing a sample, the parameter estimation error is improved by $1/\sqrt{N}$ beyond what can be achieved using a single particle. This is known as the standard quantum limit (SQL) [4]. It was shown that the best possible measurement strategy with N particles is by using quantum-correlated, i.e., entangled, states. This leads to a $1/N$ improvement in estimation error [4], an optimum that is called the Heisenberg limit (HL) [5]. For instance, in the case of an interferometric parameter estimation using photons, the multi-photon states at wavelength λ exhibit features described by the de Broglie wavelength λ/N [6–8]. Therefore, the uncertainty on the estimation of the phase scales with $1/N$. Those ideas were extended from longitudinal to transverse interference patterns. Quantum lithography was proposed where entangled photon number states, so called NOON states, show a λ/N resolution improvement in transverse interference patterns. A two-fold narrower diffraction pattern compared to classical light with the same wavelength was observed by placing a double slit immediately after a spontaneous parametric down-conversion source [9]. Furthermore, a Heisenberg limited lithographic imaging scheme based on reciprocal binomial states was proposed in [10]. Transverse interference fringes at the HL were further shown by combining temporally shaped classical light and nonlinear multi-photon absorber systems for detection [11–13].

The tools of quantum metrology can be applied to imaging, i.e., the transmission of object shape information to an image plane. By doing so, the uncertainty on a parameter estimation is replaced by the concept of image resolution. Classically, the wavelength λ of the used illumination and the numerical aperture (NA) of the imaging system determine the image resolution through the Rayleigh resolution limit $1.22\lambda/\mathrm{NA}$ [14]. However, a more quantitative definition of the resolution should take into account both the optical system resolution and the noise on the measured signal. Recently, the concept of Fisher information has thrown new light on the Rayleigh limit by theoretically quantifying the amount of information in measurements of two separated incoherent point sources [15,16]. Using quantum metrology concepts, it has been possible to experimentally implement optimal measurements, allowing to effectively resolve the two point sources below the Rayleigh limit [17–20].

For arbitrary objects, quantum imaging makes use of quantum states of light to go beyond the Rayleigh limit [21]. Extending the concept of a photon's de Broglie wavelength to imaging, N-photon imaging schemes have been proposed towards reducing the effective resolving power of optical systems by $\sqrt{N}$, corresponding to the SQL, or even by N, the HL [22]. It has to be noted that the final resolution depends both on the resolving power and on the shot noise that scales with $1/\sqrt{M}$, where M is the number of measurements. Schemes such as ghost

imaging [3,23] or thermal light imaging [23,24] rely on classical correlations and therefore cannot achieve improvement beyond the SQL. In a standard imaging setup, only changing the illumination to a spatially entangled light source, the SQL cannot be beaten [25–27]. In order to reach the HL, specific schemes are to be designed [22].

Despite these advances, no actual imaging of object features at the HL has been performed yet. One reason is the lack of N-photon transmitters. These are shown in [22] to allow for imaging at the HL but can be omitted by preparing a quantum state that would be fully transmitted by such a device, as realized in this work. Time-consuming scanning or iteration in generation of the optical states to build up image structures in the aforementioned schemes prevented their application. Our experimental implementation of the state generation operates in a single-shot mode. Moreover, quantum imaging was hindered by the low speed of correlation measurements using scanning single-pixel devices. A recently developed integrated sub-nanosecond time-resolving 2D detector array allows for fast correlation measurements without scanning [28].

Schemes related to quantum lithography require coincidence detection of the photons at the same position, which is highly inefficient. The detection efficiency is strongly enhanced by the method of optical centroid measurement (OCM) Tsang presented in [29]. The OCM method allows transmission of the centroid position of a monochromatic spatially entangled N-photon state beyond the Rayleigh diffraction limit. OCM was experimentally implemented in [30] for photon number $N = 2$ and in [31] for $N = 2$ to 4. Both implementations demonstrated super-resolution at the HL by measuring oscillation periods of far-field interference fringes of two plane waves.

In this work, the OCM method is used in an imaging setting where, instead of far-field interference fringes, actual object near-field features are observed. (The paper is accompanied by Supplement 1 that additionally shows an OCM far-field diffraction pattern of a double slit.) The OCM theory is derived in an imaging formalism. Moreover, coherent OCM imaging is implemented for photon number $N = 2$, where an experimental setup is presented that allows us to generate an entangled biphoton state containing the super-resolved OCM image.

2. THEORY

An object can be described by its transmission aperture function $A(\boldsymbol{\rho})$ in the transverse position coordinates $\boldsymbol{\rho} = (x, y)$. For a monochromatic, spatially coherent, and uniform light source at wavelength λ, the electric field after the object becomes $E(\boldsymbol{\rho}) \propto A(\boldsymbol{\rho})$. The goal of an imaging system is to reproduce the object field distribution in a distant plane, where it can be measured or exposes a film. For a coherent imaging system, the field intensity in the image plane reads

$$I(\boldsymbol{\rho}) = \left| \int \mathrm{d}^2\boldsymbol{\rho}'\; A(\boldsymbol{\rho}')h\left(\frac{\boldsymbol{\rho}}{m} - \boldsymbol{\rho}'\right)\right|^2 = \left|(A * h)\left(\frac{\boldsymbol{\rho}}{m}\right)\right|^2, \quad (1)$$

with magnification m and the point-spread function (PSF) $h(\boldsymbol{\rho})$ being specific to that system and used wavelength [14,23]. A translation-invariant PSF is assumed. Image resolution can then be defined by the width of the PSF, and an optimal image is achieved with $h(\boldsymbol{\rho}) = \delta^{(2)}(\boldsymbol{\rho})$.

In order to transmit with an imaging system object features below the size of its PSF, i.e., the Rayleigh limit, Tsang proposed to replace the classical field distribution at the object plane by quantum-correlated multi-photon states [29]. From these results, an explicit state can be constructed. For the case of a coherent image of the object $A(\boldsymbol{\rho})$ and N photons at wavelength λ, the OCM image state reads

$$|\Psi\rangle = \int \mathrm{d}^2\boldsymbol{\rho}_1 \ldots \mathrm{d}^2\boldsymbol{\rho}_N\; A\left(\frac{\boldsymbol{\rho}_1 + \ldots + \boldsymbol{\rho}_N}{N}\right)|\boldsymbol{\rho}_1, \ldots, \boldsymbol{\rho}_N\rangle \quad (2)$$

in transverse positions of the photons $\boldsymbol{\rho}_1, \ldots, \boldsymbol{\rho}_N$. Introducing new coordinates further simplifies analysis. The centroid position $\boldsymbol{X}$ and the deviations $\boldsymbol{\xi}_k$ are defined by

$$\boldsymbol{X} := \frac{1}{N}\sum_{k=1}^{N}\boldsymbol{\rho}_k, \qquad \boldsymbol{\xi}_k := \boldsymbol{\rho}_k - \boldsymbol{X}, \qquad k \in \{1, \ldots, N\}.$$

Due to $\sum_k \boldsymbol{\xi}_k = 0$, the N-tuple $(\boldsymbol{X}, \boldsymbol{\xi}_1, \ldots, \boldsymbol{\xi}_{N-1})$ forms a complete coordinate system. In these coordinates, the quantum state encodes the image in the centroid position $\boldsymbol{X}$. Notice the infinite extension of the state in all $\boldsymbol{\xi}_k$ coordinates in this optimal case.

Propagating the electric field from the object plane through the imaging system, the N-photon detection probability density in the image plane is given by the Nth order correlation function [32]

$$G^{(N)}(\boldsymbol{\rho}_1, \ldots, \boldsymbol{\rho}_N) = \left| \int \mathrm{d}^2\boldsymbol{\rho}'_1 \ldots \mathrm{d}^2\boldsymbol{\rho}'_N A(\boldsymbol{X}') \right.$$
$$\left. h\left(\frac{\boldsymbol{\rho}_1}{m} - \boldsymbol{\rho}'_1\right)\ldots h\left(\frac{\boldsymbol{\rho}_N}{m} - \boldsymbol{\rho}'_N\right)\right|.$$

A change to the coordinates $\boldsymbol{X}$ and $\boldsymbol{\xi}_k$ with $k \in \{1, \ldots, N-1\}$ leads to

$$G^{(N)}(\boldsymbol{X}, \boldsymbol{\xi}_1, \ldots, \boldsymbol{\xi}_{N-1}) = \left|(A * H)\left(\frac{\boldsymbol{X}}{m}\right)\right|^2, \quad (3)$$

where the centroid PSF is given by the N-times repeated self-convolution

$$H(\boldsymbol{X}) = N^2(\underbrace{h * \ldots * h}_{\times N})(N\boldsymbol{X}) \quad (4)$$

and determines the resolution of the image in the centroid coordinate $\boldsymbol{X}$; see Section 1 in Supplement 1. As formally explicit in comparison to Eq. (1), the image is formed coherently. With an appropriate mixed state, an incoherent imaging variant is derived in Section 2 in Supplement 1. Summing $G^{(N)}$ over the $\boldsymbol{\xi}_k$ coordinates in dependence of the $\boldsymbol{X}$ coordinate yields the 2D image.

In the following, we consider for the imaging system a single lens with a circular pupil of radius R determining its NA and Rayleigh resolution limit. The PSF is then given by a jinc function $h(\boldsymbol{\rho}) = \mathrm{jinc}(2\pi R|\boldsymbol{\rho}|/s_o\lambda)$ with the distance s_o from the object plane to the lens [14,23]. The jinc function is defined as $\mathrm{jinc}(x) = 2J_1(x)/x$, with J_1 being the first-order Bessel function [14], and it is also known as the sombrero function [23]. By assuming $s_o \gg |\boldsymbol{\rho}|^2/\lambda$ for $\boldsymbol{\rho}$ in the object and detector area, the phase $\exp(i\pi|\boldsymbol{\rho}|^2/\lambda s_o)$ appearing in the object plane for single-lens imaging can be neglected. This establishes the translation invariance of the PSF. Using Eq. (4), it can be shown that

$$H(\boldsymbol{X}) = C\;\mathrm{jinc}\left(\frac{2\pi RN}{s_o\lambda}|\boldsymbol{X}|\right), \quad (5)$$

with an appropriate normalization constant C; see Section 1 in Supplement 1. The additional factor of N in the argument

reduces the width of the PSF, leading to a spatial resolution enhancement corresponding to a HL $1/N$ scaling in photon number.

For discussing the mechanism of resolution enhancement, it is of value to determine the photon correlations in the plane of the lens pupil. Assuming s_o to be large, correlations in the far field can be considered. The OCM state of Eq. (2) in a far-field basis is given by

$$|\Psi\rangle = \int \mathrm{d}^2\boldsymbol{q}\tilde{A}(N\boldsymbol{q})|\boldsymbol{q},\ldots,\boldsymbol{q}\rangle, \tag{6}$$

where $\tilde{A}(\boldsymbol{q})$ is the Fourier transform of $A(\boldsymbol{\rho})$ in the transverse wave vector coordinate $\boldsymbol{q}$. This coordinate can be related to a position in the pupil plane by $\boldsymbol{\rho} = (s_o\lambda/2\pi)\boldsymbol{q}$ in paraxial approximation [14]. Strong position correlation is therefore present at the pupil.

3. EXPERIMENT

Our proof-of-principle experiment generates an OCM state for photon number $N = 2$. Combined with a low-NA single-lens imaging, its spatial resolution capability can be assessed and compared to theory and classical light sources. The optical setup for the preparation of the OCM state given in Eq. (2) with $N = 2$ is depicted in Fig. 1. An object aperture $A(\boldsymbol{\rho})$ is illuminated by a continuous-wave (CW) pump laser at 405 nm and 30 mW in the plane Σ_o'. A $4f$ lens system consisting of two lenses L_1 and L_2 of focal length $f = 50$ mm images the object to the preparation output plane Σ_o. In the far-field plane between the lenses, a 5 mm long periodically poled $KTiOPO_4$ nonlinear crystal (NLC) generates photon pairs in type-0, frequency-degenerate, collinear spontaneous parametric down-conversion (SPDC). This emission is spectrally filtered by a band-pass filter (BP) transmitting $\lambda = 810 \pm 5$ nm.

Using the approximation of a thin crystal and a plane-wave pump, the entangled biphoton state in the output plane Σ_o is derived in [32] and is given by Eq. (2) for $N = 2$. In the thick crystal case, it can be shown to read

$$|\Psi\rangle = \int \mathrm{d}^2\boldsymbol{\rho}_1\mathrm{d}^2\boldsymbol{\rho}_2 A\left(-\frac{\boldsymbol{\rho}_1+\boldsymbol{\rho}_2}{2}\right)\mathrm{sinc}\left(\frac{\Delta kL}{2}\right)|\boldsymbol{\rho}_1,\boldsymbol{\rho}_2\rangle, \tag{7}$$

with the NLC length L and wave vector mismatch $\Delta k(\boldsymbol{q}_1,\boldsymbol{q}_2)$ evaluated at $\boldsymbol{q}_k = (2\pi/\lambda f)\boldsymbol{\rho}_k, k \in \{1,2\}$; see the full derivation in Section 3 of Supplement 1. The mentioned infinite extension of the ideal OCM state in Eq. (2) is here restricted by the dependence of this phase-matching function on $\boldsymbol{\xi}_1 = (\boldsymbol{\rho}_1 - \boldsymbol{\rho}_2)/2$.

The resolution-limited imaging is performed from Σ_o to the image plane Σ_i with lens L_3 of 250 mm focal length at a distance $s_o = 355$ mm between Σ_o and the lens. With the given detector and object sizes, the assumption of a large s_o in the theory section is valid. A magnification of $m = 2.4$ is measured. A circular pupil of radius $R = 1.38$ mm in front of the lens limits the NA.

For resolution comparison, the classical light sources are spatially coherent monochromatic illumination at 405 nm and 810 nm as well as spatially incoherent light at 810 nm. The former are implemented using collimated lasers, the latter by a halogen incandescent lamp spectrally filtered at 810 ± 5 nm. For imaging with classical light, the setup of Fig. 1 is used unaltered and allows comparison with otherwise identical parameters.

The newly developed detector used in the image plane Σ_i is an integrated, fully digital 32×32 pixel sensor array with single-photon sensitivity manufactured in CMOS technology [28].

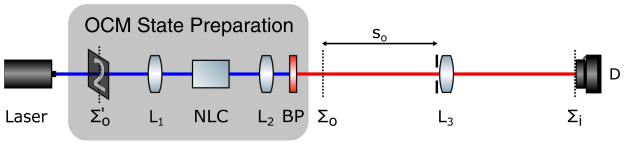

Fig. 1. Optical setup consisting of OCM state preparation and single-lens imaging (right). A 405 nm laser source illuminates an object in the plane Σ_o'. $4f$ imaging from Σ_o' to the output plane Σ_o is performed by lenses L_1 and L_2. The nonlinear crystal (NLC) in the central far-field plane produces photon pairs in SPDC. A band-pass filter (BP) transmits at 810 nm. Resolution-limited imaging is performed by the low-NA lens L_3 from output plane Σ_o to image plane Σ_i, where the 2D detector array D measures correlations.

The size of the pixel being smaller than the PSF of the optical system is thus not limiting the resolution. This device contains for every pixel a dedicated time-to-digital converter that time-stamps the first detection event at 205 ps resolution in a frame of 45 ns duration. At an observation rate of 800 kHz, a measurement duty-cycle of 3.6% is achieved. The photon detection efficiency reaches 5% at 400 nm and 0.8% at 810 nm. Covering a sensitive region of 1.4×1.4 mm^2, the sensor is capable of efficiently measuring second-order correlation functions similarly to its predecessor presented in [33]. Despite that these types of devices have existed since 2009 [28], their use in quantum optics applications have been limited by low a fill factor (1%–5%). Only recently has it been possible to achieve 19.48%, allowing useful detection efficiencies [28]. For this work, a coincidence window of 1 ns is used where accidental events, including all dark counts, can be measured and removed.

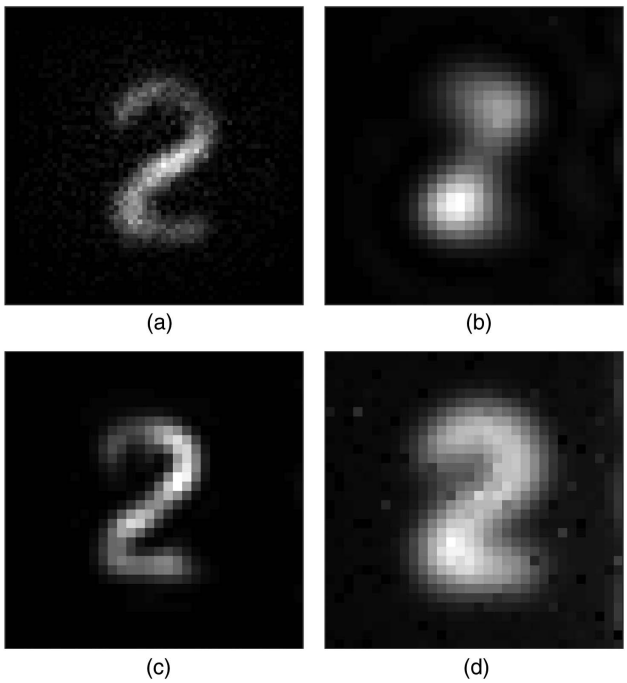

Fig. 2. Imaging of an object using a single lens with different illumination light sources: Biphoton OCM at 810 nm (a), spatially coherent laser at 810 nm (b) and 405 nm (c), spatially incoherent light at 810 nm (d). The same low NA is used to demonstrate the wavelength dependence of the resolution. The region of 1.4×1.4 mm^2 is acquired by a 32×32 pixels sensor. Biphoton OCM yields images at half-pixels and achieves a comparable image resolution at 810 nm to that of a coherent light at 405 nm.

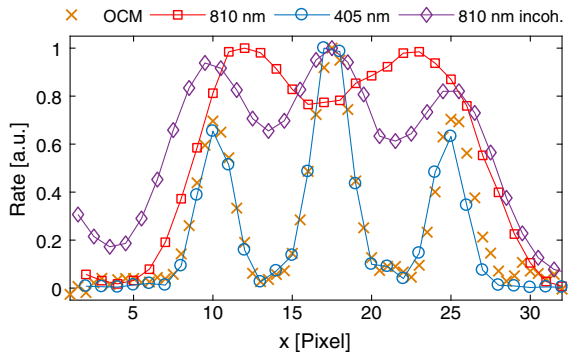

Fig. 3. Triple-slit object of 70 μm linewidth is used for resolution comparison. Cross sections in low-NA imaging using biphoton OCM at 810 nm (crosses), spatially coherent illumination at 810 nm (squares) and 405 nm (circles), and incoherent light at 810 nm (diamonds) are shown. OCM shows an advantage that is practically identical to the double resolution given with 405 nm.

In Figs. 2(a)–2(d), a 200 × 300 μm^2 object aperture is imaged at low NA values with different light sources. In the case of OCM, the measurement of the full second-order correlation function of Eq. (3) yields the image of Fig. 2(a) by summing over $\boldsymbol{\xi}_1$. Because the image is encoded in the centroid position, the image can be reconstructed at half-pixel precision, leading to 63 × 63 pixels images acquired by the 32 × 32 pixels sensor. In order to suppress detector crosstalk between adjacent pixels, only events with $|\boldsymbol{\xi}_1| >$ 1 pixel are considered. A measurement time of 10 h is used in Fig. 2(a).

For a more objective comparison, cross-sections of a triple-slit object of 70 μm line width imaged at low NA are shown in Fig. 3. OCM imaging resolution surpasses coherent and incoherent light at 810 nm and shows practically identical resolution as 405 nm. Imaging a point of 25 μm Gaussian waist radius realized by focusing the pump laser and classical light sources in the object plane Σ_o', the PSF of the single-lens imaging at low NA is compared in Fig. 4. The theoretical curves for classical imaging are given by Eq. (1) and the classical PSF of Eq. (5) with $N = 1$. Classically correlated photon pairs of OCM type would produce a centroid PSF $|H(\boldsymbol{X})|^2 = (|h|^2 * |h|^2)(2\boldsymbol{X})$; see Section 4 in Supplement 1. This distribution is shown for comparison (dashed line) and scales at the SQL. This limit is surpassed by the OCM PSF and thereby verifies the quantum correlation nature of the enhancement. Far-field measurements confirm the theoretical prediction of Eq. (6); see Section 5 in Supplement 1.

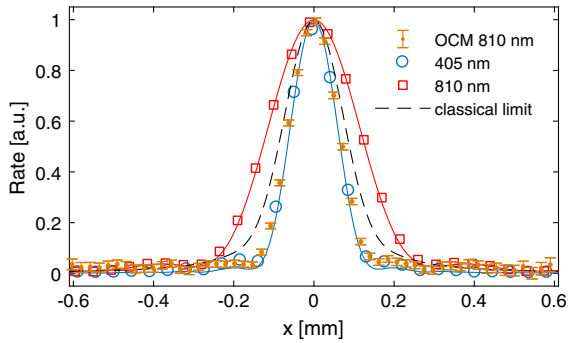

Fig. 4. Projection of the PSF of low-NA single-lens imaging at different light sources. Measurements with coherent light at 810 nm (squares) and 405 nm (circles) are shown with their theoretical curves. The biphoton OCM PSF at 810 nm (dots) closely agrees with 405 nm and confirms its doubled resolution. Statistical 2σ errors are shown. The OCM PSF surpasses a theoretical SQL-scaling PSF of the centroid of two classically correlated photons at 810 nm (dashed line).

4. DISCUSSION

In contrast to resolution enhancement techniques by image post-processing or correlation measurements in quantum microscopy [3], the quantum state of light, as generated here, physically carries a spatial structure surpassing the Rayleigh limit. The mechanism giving rise to the super-resolution can be understood by considering the far-field correlations of the OCM state. As evident in Eq. (6), it shows strong wave vector correlations or, equivalently, position correlations in the pupil plane. This situation can be regarded as a multi-mode NOON state emanating from the lens and propagating to the image plane. As shown in [30,31] for two-mode NOON states, this leads to N-times narrower multi-photon interference fringes in the image plane. The multi-mode case presented here allows us to build up an image by the coherent superposition of such fringes of different directions and sizes.

With the current SPDC sources of entangled photons, the method of generating the OCM state presented in this paper is the most efficient. To avoid the separation between state generation and imaging, a thin NLC could be placed directly at the imaging lens covering the full pupil area—at the price, however, of lower efficiency. For reaching a larger photon number N, higher-order nonlinear effects should be used [34].

Furthermore, the nonlinearity needed to generate entanglement could, in principle, take place in the optical setup instead of the source. For instance, as previously mentioned, super-resolution can be achieved by using a spatially correlated light source for illuminating the object and using a N-photon transmitter (NPT) in front of the imaging lens [22]. Such devices would transmit spatially correlated N-photon states only, maintaining the N-photon coherence. Effectively, this filtering projects the incoming state to Eq. (6) or its incoherent imaging analogue and would therefore create an OCM state in the image plane. This general principle can be extended to an optical system of many lenses, where a NPT is placed at every lens. Intuitively, this mimics the propagation of a single photon of the de Broglie wavelength by forcing all N photons to stay together and trace the same paths. As efficient NPTs are yet not practically available, another approach was proposed in [23] for $N = 2$. The object is illuminated by spatially correlated biphoton light. Ultra-fast temporal quantum correlations of the pair are used through their relative time of arrival in the image plane to post-select on correlated positions on the lens pupil, where both photons take the same path, thus enabling resolution at the HL. It still has to be analyzed how temporal and spatial resolution are related and how to extend this scheme to higher values of N.

In conclusion, our theoretical and experimental results demonstrate the possibility to engineer quantum states of light that physically carry a super-resolved spatial structure at the HL. This is investigated in low-NA single-lens imaging, where spatial resolution is compared across different light sources. The OCM biphoton state shows an enhancement close to a factor of 2 corresponding to a Rayleigh resolution at its de Broglie wavelength. For high-NA systems, where the classical resolution is mainly

limited by the wavelength, or for higher photon number N, theory suggests the possibility to see sub-wavelength features. A full vectorial field analysis in contrast to the scalar approximations has yet to show the advantage in this limit.

The results presented here were made possible by the development of an integrated single-photon detector array, although the present device has non-optimal detection efficiency at the used wavelength. By optimizing the design and increasing the number of pixels, CMOS detectors will certainly be key components of any future applications in the field of quantum imaging.

As elaborated by Tsang in [29] and shown here, the image acquisition efficiency of the OCM correlations is very high due to the fact that every N-photon event carries image information. In the case of an N-photon absorbing film in lithography, where only spatially coincident events ($\xi_k = 0, k \in \{1, \ldots, N\}$) are registered, the image would be reproduced at N-fold resolution but at an efficiency that is expected to drop exponentially with N [22]. Efficiency can be gained by loosening the condition of strong correlation in the far field. An analysis of resolution and efficiency versus correlation length and photon number has yet to be performed.

The theory developed here is general and allows for different experimental realizations. As a concrete example, the presented biphoton experiment serves as a proof of concept, agreeing to the theory and showing its advantage over classical light sources. Moreover, by unifying the understanding of recent results aiming at super-resolution at the HL, it might stimulate new paths of research.

Funding. Schweizerischer Nationalfonds zur Förderung der Wissenschaftlichen Forschung (SNF) (PP00P2_159259); H2020 Future and Emerging Technologies (FET) (686731).

Acknowledgment. We thankfully acknowledge the support of the European Commission through the SUPERTWIN project. This research was supported by the Swiss National Science Foundation.

See Supplement 1 for supporting content.

REFERENCES

1. K. T. Kapale, L. D. Didomenico, H. Lee, P. Kok, and J. P. Dowling, "Quantum interferometric sensors," Proc. SPIE **6603**, 660316 (2007).
2. V. Giovannetti, S. Lloyd, and L. Maccone, "Advances in quantum metrology," Nat. Photonics **5**, 222–229 (2011).
3. D. Simon, G. Jaeger, and A. Sergienko, *Quantum Metrology, Imaging, and Communication*, Quantum Science and Technology (Springer International, 2016).
4. V. Giovannetti, S. Lloyd, and L. Maccone, "Quantum metrology," Phys. Rev. Lett. **96**, 010401 (2006).
5. Z. Y. Ou, "Fundamental quantum limit in precision phase measurement," Phys. Rev. A **55**, 2598–2609 (1997).
6. J. Jacobson, G. Björk, I. Chuang, and Y. Yamamoto, "Photonic de Broglie waves," Phys. Rev. Lett. **74**, 4835–4838 (1995).
7. K. Edamatsu, R. Shimizu, and T. Itoh, "Measurement of the photonic de Broglie wavelength of entangled photon pairs generated by spontaneous parametric down-conversion," Phys. Rev. Lett. **89**, 213601 (2002).
8. T. Nagata, R. Okamoto, J. L. O'Brien, K. Sasaki, and S. Takeuchi, "Beating the standard quantum limit with four-entangled photons," Science **316**, 726–729 (2007).
9. M. D'Angelo, M. V. Chekhova, and Y. Shih, "Two-photon diffraction and quantum lithography," Phys. Rev. Lett. **87**, 013602 (2001).
10. G. Björk, L. L. Sánchez-Soto, and J. Söderholm, "Entangled-state lithography: tailoring any pattern with a single state," Phys. Rev. Lett. **86**, 4516–4519 (2001).
11. E. Yablonovitch and R. B. Vrijen, "Optical projection lithography at half the Rayleigh resolution limit by two-photon exposure," Opt. Eng. **38**, 334–338 (1999).
12. A. Pe'er, B. Dayan, M. Vucelja, Y. Silberg, A. A. Friesem, Y. Silberberg, A. A. Friesem, Y. Silberg, and A. A. Friesem, "Quantum lithography by coherent control of classical light pulses," Opt. Express **12**, 6600–6605 (2004).
13. P. R. Hemmer, A. Muthukrishnan, M. O. Scully, and M. S. Zubairy, "Quantum lithography with classical light," Phys. Rev. Lett. **96**, 163603 (2006).
14. J. Goodman, *Introduction to Fourier Optics*, McGraw-Hill Physical and Quantum Electronics Series (W. H. Freeman, 2005).
15. M. Tsang, R. Nair, and X.-M. Lu, "Quantum theory of superresolution for two incoherent optical point sources," Phys. Rev. X **6**, 031033 (2016).
16. C. Lupo and S. Pirandola, "Ultimate precision bound of quantum and subwavelength imaging," Phys. Rev. Lett. **117**, 190802 (2016).
17. M. Paúr, B. Stoklasa, Z. Hradil, L. L. Sánchez-Soto, and J. Rehacek, "Achieving the ultimate optical resolution," Optica **3**, 1144–1147 (2016).
18. Z. S. Tang, K. Durak, and A. Ling, "Fault-tolerant and finite-error localization for point emitters within the diffraction limit," Opt. Express **24**, 22004–22012 (2016).
19. W.-K. Tham, H. Ferretti, and A. M. Steinberg, "Beating Rayleigh's curse by imaging using phase information," Phys. Rev. Lett. **118**, 070801 (2017).
20. F. Yang, A. Tashchilina, E. S. Moiseev, C. Simon, and A. I. Lvovsky, "Far-field linear optical superresolution via heterodyne detection in a higher-order local oscillator mode," Optica **3**, 1148–1152 (2016).
21. M. Genovese, "Real applications of quantum imaging," J. Opt. **18**, 073002 (2016).
22. V. Giovannetti, S. Lloyd, L. Maccone, and J. H. Shapiro, "Sub-Rayleigh-diffraction-bound quantum imaging," Phys. Rev. A **79**, 013827 (2009).
23. Y. Shih, "Quantum imaging," IEEE J. Sel. Top. Quantum Electron. **13**, 1016–1030 (2007).
24. J.-E. Oh, Y.-W. Cho, G. Scarcelli, and Y.-H. Kim, "Sub-Rayleigh imaging via speckle illumination," Opt. Lett. **38**, 682–684 (2013).
25. I. F. Santos, J. G. Aguirre-Gómez, and S. Pádua, "Comparing quantum imaging with classical second-order incoherent imaging," Phys. Rev. A **77**, 043832 (2008).
26. F. Guerrieri, L. Maccone, F. N. C. Wong, J. H. Shapiro, S. Tisa, and F. Zappa, "Sub-Rayleigh imaging via N-photon detection," Phys. Rev. Lett. **105**, 163602 (2010).
27. D.-Q. Xu, X.-B. Song, H.-G. Li, D.-J. Zhang, H.-B. Wang, J. Xiong, and K. Wang, "Experimental observation of sub-Rayleigh quantum imaging with a two-photon entangled source," Appl. Phys. Lett. **106**, 171104 (2015).
28. L. Gasparini, M. Zarghami, H. Xu, L. Parmesan, M. M. Garcia, M. Unternährer, B. Bessire, A. Stefanov, D. Stoppa, and M. Perenzoni, "A 32 × 32-pixels time-resolved single-photon image sensor with 44.64-μm pitch and 19.48% fill-factor with on-chip row/frame skipping features reaching 800 kHz observation rate for quantum physics applications," in *International Solid-State Circuits Conference (ISSCC)* (IEEE, 2018).
29. M. Tsang, "Quantum imaging beyond the diffraction limit by optical centroid measurements," Phys. Rev. Lett. **102**, 253601 (2009).
30. H. Shin, K. W. C. Chan, H. J. Chang, and R. W. Boyd, "Quantum spatial superresolution by optical centroid measurements," Phys. Rev. Lett. **107**, 083603 (2011).
31. L. A. Rozema, J. D. Bateman, D. H. Mahler, R. Okamoto, A. Feizpour, A. Hayat, and A. M. Steinberg, "Scalable spatial superresolution using entangled photons," Phys. Rev. Lett. **112**, 223602 (2014).
32. A. Abouraddy, B. E. A. Saleh, A. V. Sergienko, and M. C. Teich, "Entangled-photon Fourier optics," J. Opt. Soc. Am. B **19**, 1174–1184 (2002).
33. M. Unternährer, B. Bessire, L. Gasparini, D. Stoppa, and A. Stefanov, "Coincidence detection of spatially correlated photon pairs with a monolithic time-resolving detector array," Opt. Express **24**, 28829–28841 (2016).
34. M. Corona, K. Garay-Palmett, and A. B. U'Ren, "Experimental proposal for the generation of entangled photon triplets by third-order spontaneous parametric downconversion in optical fibers," Opt. Lett. **36**, 190–192 (2011).